Intrinsic axion insulating behavior in antiferromagnetic MnBi$_6$Te$_{10}$

Na Hyun Jo[1,2,*] Lin-Lin Wang [1,†] Robert-Jan Slager,[3,‡] Jiaqiang Yan,[4] Yun Wu,[1,2] Kyungchan Lee,[1,2]
Benjamin Schrunk [1,2] Ashvin Vishwanath,[3,§] and Adam Kaminski[1,2,‖]

[1]*Ames Laboratory, Iowa State University, Ames, Iowa 50011, USA*
[2]*Department of Physics and Astronomy, Iowa State University, Ames, Iowa 50011, USA*
[3]*Department of Physics, Harvard University, Cambridge, Massachusetts 02138, USA*
[4]*Materials Science and Technology Division, Oak Ridge National Laboratory, Oak Ridge, Tennessee 37831, USA*

A striking feature of time-reversal symmetry (TRS) protected topological insulators (TIs) is that they are characterized by a half integer quantum Hall effect on the boundary when the surface states are gapped by time-reversal breaking perturbations. While TRS-protected TIs have become increasingly under control, magnetic analogs are still a largely unexplored territory with novel rich structures. In particular, magnetic topological insulators can also host a quantized axion term in the presence of lattice symmetries. Since these symmetries are naturally broken on the boundary, the surface states can develop a gap without external manipulation. In this paper, we combine theoretical analysis, density-functional calculations and experimental evidence to reveal intrinsic axion insulating behavior in MnBi$_6$Te$_{10}$. The quantized axion term arises from the simplest possible mechanism in the antiferromagnetic regime where it is protected by inversion symmetry and the product of a fractional translation and TRS. The anticipated gapping of the Dirac surface state at the edge is subsequently experimentally established using angle resolved photoemission spectroscopy (ARPES). As a result, this system provides the magnetic analog of the simplest TRS-protected TI with a single, gapped Dirac cone at the surface.

I. INTRODUCTION

Topology has drastically changed our understanding of insulators and metals. One of the most intriguing consequences of topological materials is that they allow for the realization of exotic quasiparticles and phases in real materials in the laboratory. A prime example in this regard is that topological insulators (TIs) provide for the condensed-matter realization of the θ vacuum [1,2], meaning that the electromagnetic response is governed by a term

$$S_{\text{axion}} = \theta \frac{\alpha}{(4\pi^2)} \int d^3x dt\, \mathbf{E} \cdot \mathbf{B}, \qquad (1)$$

where $\alpha = e^2/(\hbar c)$ refers to the fine-structure constant. This term is manifested through the topological magnetoelectric effect (TME), having profound consequences [1–3]. In particular, the response coefficient is quantized to odd numbers of the fine-structure constant $\alpha = e^2/(\hbar c)$ divided by 4π. Being a total derivative, the TME finds its physical origin by considering the edge. Here, its presence results in a half-quantized anomalous Hall conductivity, which essentially corresponds to the odd number of Dirac fermions on the surface [1]. The exotic nature of the TME also has been associated with other proposals, such as inducing a magnetic monopole upon bring-

ing electric charge close to the surface [4], which in some scenarios is proposed to allow for the formation of the condensed-matter variant of the elusive dyon excitation [5] as well as magneto-optical Faraday and Kerr rotation effects [6–9].

While upon gapping the surface states of 3D time-reversal symmetry (TRS)-protected TIs, having $\theta = \pi$, the TME can be accessed, this requires intricate external manipulation. On the other hand, magnetism cannot only induce topological structures [10] that are yet to be fully explored but may give rise to axion and quantum anomalous Hall effects *intrinsically* [11,12]. In particular, the presence of lattice symmetries, such as fractional translations combined with TRS, or inversion symmetry, can also give rise to a quantized axion angle, $\theta = \pi$. As surface terminations will generally break these symmetries, the associated gapless states of such magnetic TIs are naturally gapped without the need for complicated external manipulation. As a result, such systems provide a natural platform for the aforementioned physical effects. Finally, magnetic domain walls of magnetic TIs can host conducting modes, making them an exciting platform to study in their own right [13].

Recently, it was predicted that this physics can be realized in MnBi$_2$Te$_4$ [14,15]. Subsequently, single crystals of MnBi$_{2n}$Te$_{3n+1}$ were grown and physical properties, including electrical and thermal transport, magnetization, neutron scattering, etc., were measured which support possible realization of the axion insulator in these materials [16–21]. While some ARPES studies reported observation of a gapped surface state in MnBi$_{2n}$Te$_{3n+1}$ and thus possible axion insulator behavior [22–25], many others showed evidence that the surface state in this material remains gapless or diminished gap down

to low temperatures [26–30]. The latter may be a result of weak hybridization between the magnetic states and the topological electronic states [30] or possibly a different (or disordered) magnetic structure at the top Mn-Te layer [26,28].

In this paper, we report theoretical understanding and experimental evidence of intrinsic axion insulating behavior in a different but related material, $MnBi_6Te_{10}$ with A-type antiferromagnetic (AFM) order, having a reported bulk transition temperature of $T = 11$ K [18]. $MnBi_6Te_{10}$ has a rhombohedral crystal structure ($R\bar{3}m$, 166) with repetitions of a septuple layer and two quintuple layers. The topological evaluation of the band structure is remarkably transparent, see also Appendix 2. Due to the inversion symmetry I of $R\bar{3}m$, the properties are conveniently determined by analysis of
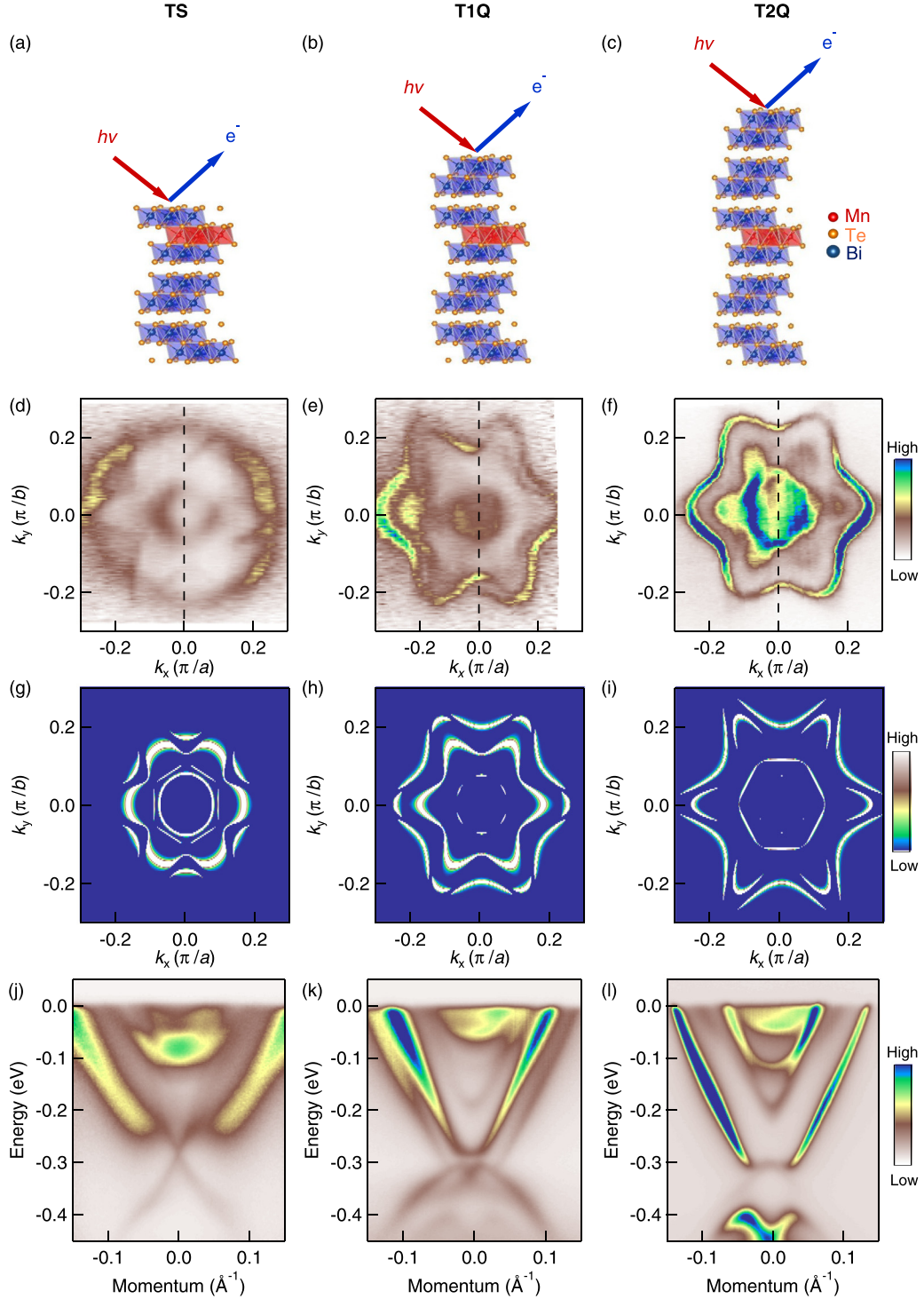

FIG. 1. Crystal structure and band structures of $MnBi_6Te_{10}$ with three different terminations. (a)–(c) Crystal structure of $MnBi_6Te_{10}$ and possible terminations, TS, T1Q, and T2Q. (d)–(f) Fermi surface plots of TS, T1Q, and T2Q terminations, respectively. (g)–(i) DFT calculations of Fermi surfaces of TS, T1Q, and T2Q terminations, respectively. (j)–(l) Band dispersions along the high symmetry lines of $k_x = 0$ of (b)–(d).

the parity eigenvalues at the time-reversal invariant momenta (TRIM) satisfying $\mathbf{k} = n_1/2\mathbf{b}_1 + n_2/2\mathbf{b}_2 + n_3/2\mathbf{b}_3$, where $\mathbf{b}_i$ comprise the reciprocal lattice vectors and n_i are integers. Generalizations of the Fu-Kane criterion [31] have not only recently proven to be powerful in the context of evaluating topological band structures [32–36] but can also reveal the presence of a theta term as well as Chern numbers [37,38].

II. MAGNETIC PHASES

In the paramagnetic phase, application of the Fu-Kane criterion [31] reveals that the system is a TRS-protected strong TI. Physically, we find that the parity even/odd $|P_z^+(\uparrow\downarrow)\rangle$ and $|P_z^+(\uparrow\downarrow)\rangle$ states invert at the Γ point due to spin-orbit coupling (SOC), leading to the TI phase. This is similar to TRS-protected TIs, such as Bi_2Se_3 and Bi_2Te_3, that exhibit a single cone at the surface [39] due to a band inversion at the Γ point, giving one odd pair in the parity evaluation.

In the AFM phase, the unit cell doubles and TRS, represented by Θ, is broken, removing the necessity of Kramers pairs. Nonetheless, a symmetry S is generated that is the product of a fractional translation, $T_{1/2} = 1/2(\mathbf{a}_1 + \mathbf{a}_2 + \mathbf{a}_3)$, and TRS, $S = \Theta T_{1/2}$. S squares to a lattice translation and thus depends on momentum [40]. Defining $\tilde{k} = T_{1/2} \cdot \mathbf{k}$, we then observe that $S^2 = -1$ for $\tilde{k} = 0$ and $S^2 = 1$ for $\tilde{k} = \pi$. Consequently, the $\tilde{k} = 0$ plane is characterized by a $\mathbf{Z}_2$ index as S acts as pseudo-TRS [40]. This fits within a generalized perspective on I-symmetric insulators, in which one evaluates half of the difference between the number of filled even-parity

n^+ and odd-parity n^- states at the TRIM Γ_i [37]:

$$\eta = 1/2 \sum_{\mathbf{k} \in \Gamma_i} (n_{\mathbf{k}}^+ - n_{\mathbf{k}}^-) \quad \text{mod } 4. \qquad (2)$$

This quantity is related to a $\mathbf{Z}_4$ index as a trivial bands can be added. Whereas the odd outcomes $\eta = 1, 3$ diagnose Weyl semimetals, $\eta = 0, 2$ can correspond to insulating phases. The difference between a trivial ($\theta = 0$) and axion ($\theta = \pi$) insulator is that the latter requires a distribution of parity eigenvalues that amounts to twice an odd integer number η [37]. Potentially, this may also correspond to a stacked Chern insulator. As explained in Appendix 2, the presence of S symmetry, however, ensures that parity eigenvalues come as pairs at TRIM, eliminating the stacked Chern insulator possibility and reducing the characterization to the anticipated $\mathbf{Z}_2$ index. Due to the single inverted pair at the Γ point, we conclude that the system is a quantized axion ($\theta = \pi$) insulator and may be regarded as the AFM analog of the simplest TRS TI with a single cone at the surface [39].

S symmetry thus rather acts as TRS, although being subtly different. As in the TRS case, the distribution of parity eigenvalues allows for determination of the $\mathbf{Z}_2$ index and edge states can be gapped when S symmetry is broken [41]. In contrast to TRS, however, this depends on the surface termination. Accordingly, we show that in natural cleavage planes in the (001) direction, a gap develops, which is associated with magnetic ordering. In contrast, S-preserving surfaces show persistent gapless edge states, see Appendix 2. We note that ferromagnets in the presence of I symmetry can similarly exhibit an axion phase, but the possibility of a
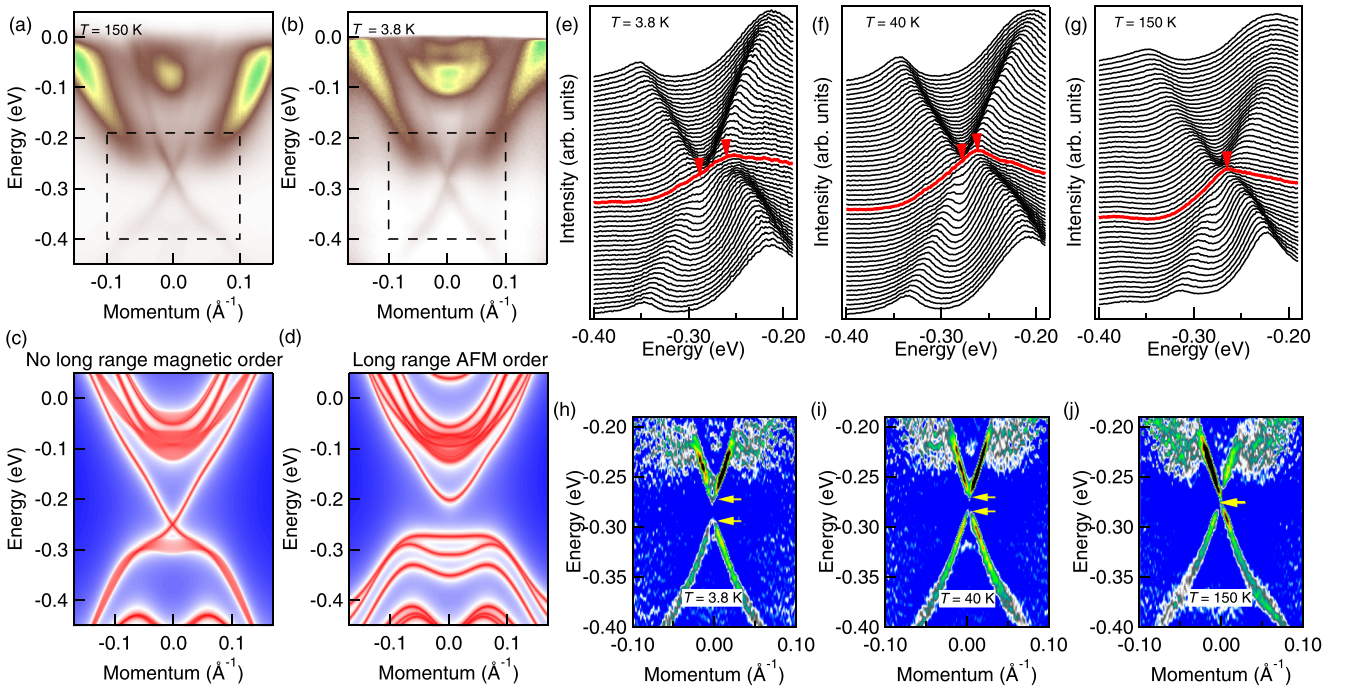

FIG. 2. Band dispersion at the TS termination. (a), (b) Band dispersions at the TS termination at $T = 150$ K and $T = 3.8$ K. (c), (d) DFT calculations of energy dispersion with no long-range magnetic order and long-range A-type AFM order, respectively. (e)–(g) EDCs corresponding to $1/2$ of the range centered $k_y = 0$ of the dashed box in a and b at 3.8, 40, and 150 K, respectively. The red curves are EDCs at the Γ point and the arrows indicate the peak positions. (h)–(j) The second derivatives of the dashed box in (a) and (b) with respect to EDC at 3.8, 40, and 150 K.

surface-preserving S symmetry makes the edge theory more versatile from the viewpoint of TME phenomena, as any termination breaks I symmetry.

III. SURFACE TERMINATION

Due to the weak van der Waals bonding between Te-Te layers, MnBi$_6$Te$_{10}$ can exfoliate above a septuple layer [TS termination, Fig. 1(a)], a quintuple layer [T1Q termination, Fig. 1(b)], and two qiuntuple layers [T2Q termination, Fig. 1(c)]. Figures 1(d)–1(f) show three different Fermi surfaces that we observed from ARPES experiments at $T = 40$ K.

We assigned the terminations based on comparison with the density-functional theory (DFT) calculations as shown in Figs. 1(g)–1(i). The determination of T1Q and T2Q terminations is clearer as we compare the energy dispersion which will be discussed later. The band dispersions along the high symmetry lines of $k_x = 0$ at $T = 40$ K corresponding to Figs. 1(d)–1(f) are shown in Figs. 1(j)–1(l), respectively. These clearly delineate the differences between each termination. For the three different terminations, nonmagnetic DFT surface band structures all give surface Dirac points (SDPs). But unlike the normal situation of TS having the SDP inside the bulk band gap between band N and N+2 (N is the number
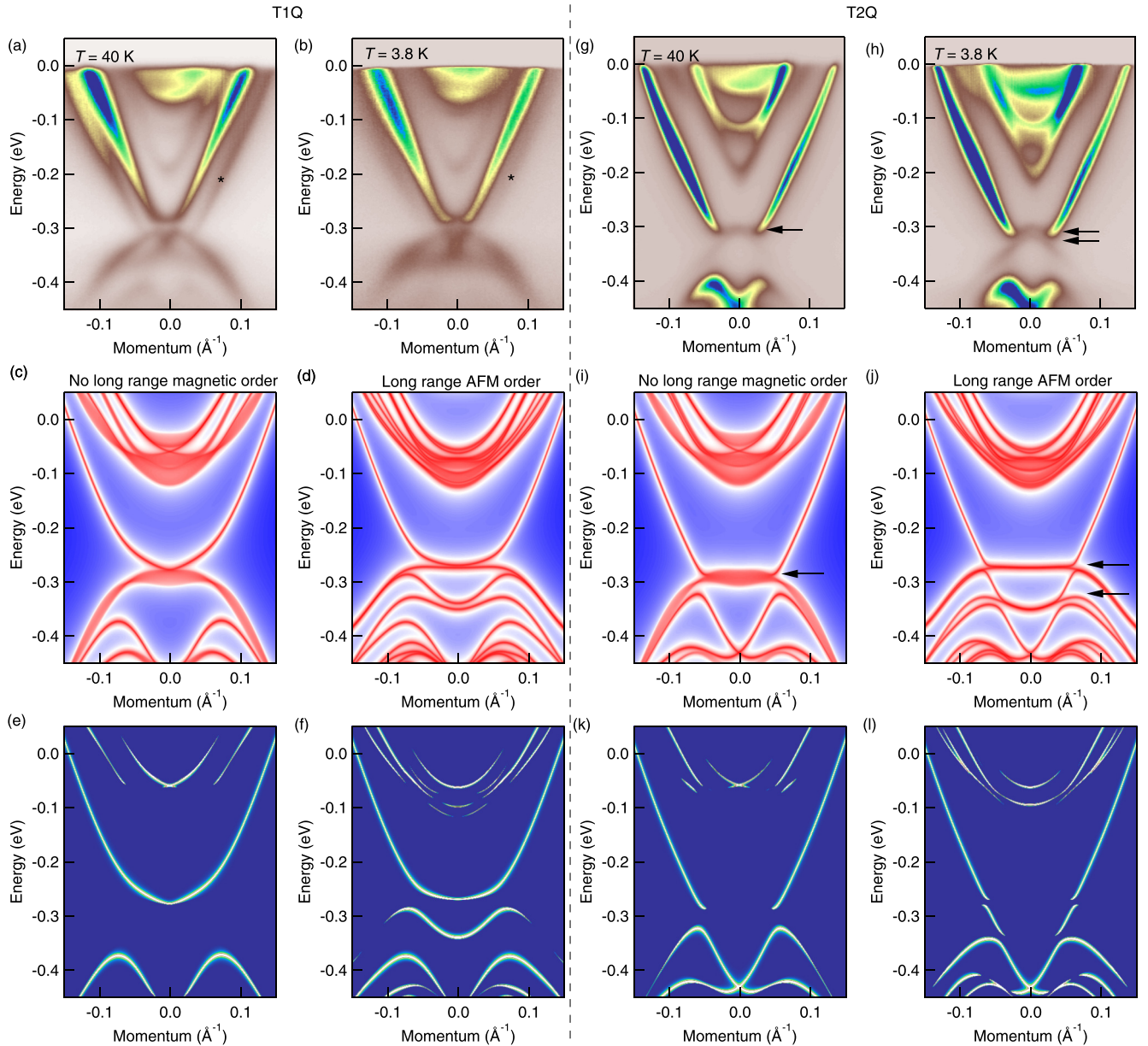

FIG. 3. Band dispersion of the T1Q and T2Q terminations. (a), (b) Band dispersions of the T1Q termination at 40, and 3.8 K. (c), (d) DFT calculations of the T1Q termination with no long-range magnetic order and long-range A-type AFM order. (e), (f) Only surface states (without bulk bands) for the T1Q termination with no long-range magnetic order and long-range A-type AFM order. (g), (h) Energy dispersions of the T2Q termination at 40, and 3.8 K. (i), (j) DFT calculations of the T2Q termination with no long-range magnetic order and long-range A-type AFM order. (k), (l) Only surface states (without bulk bands) for the T2Q termination with no long-range magnetic order and long-range A-type AFM order.

of bulk valence bands), the SDPs for T1Q and T2Q are pushed downward to be between bulk band N-2 and N. At the same time, the surface conduction bands of T1Q and T2Q merge with bulk valence bands. Similar features have also been found and discussed for $PbBi_6Te_{10}$ [42]. Furthermore, with AFM ordering in DFT surface band-structure calculations, there are gap openings for the SDPs on all three terminations as expected for breaking S symmetry on the (001) surface, but the size of gap is different. It is very small ∼1 meV on T1Q and T2Q comparing to the ∼60 meV on TS. Thus, we will focus on the gap opening of the SDP on TS below for experimentally evaluating axion behavior.

A. Temperature dependent gap in TS termination

Figure 2 presents the temperature dependence studies of the TS termination. Both ARPES data and DFT calculations show the topologically nontrivial surface states which are marked as black dashed box in Figs. 2(a) and 2(b). Although the ARPES data above and below the transition temperature [Figs. 2(a) and 2(b)] don't seem much different at the first glance, the DFT calculations suggest a clear gap forming in the ordered state (A-type AFM) with a surface gap size of ∼60 meV, which corroborates axion insulating behavior. To confirm the gap, we performed detailed spectroscopic experiments of the dashed box regime as indicated in Figs. 2(a) and 2(b). The energy distribution curves (EDCs) show a gap at $T = 3.8$ K which is below the magnetic transition temperature as shown in Fig. 2(e). The size of the surface gap is ∼30±5 meV, which is comparable to the DFT calculations. The gap still remains open at $T = 40$ K which is above the transition temperature, although the gap size is reduced compared to $T = 3.8$ K. [Fig. 2(f)] This gap finally closes at $T = 150$ K as shown in Fig. 2(g). Opening and closing of the gap can also be observed in the second derivatives in Figs. 2(h)–2(j). Note that the second derivatives are only for visualization of the presence of the gap. The discrepancy between the transition temperature and the actual temperature that the gap closes may be a result of surface magnetic fluctuation [43], meaning, that the magnetic reorientation is slower than electron scattering even in absence of the yet-to-be-formed long-range magnetic order. The actual transition temperature might also be slightly different, although the magnitude of the difference seems to suggest this is not the defining reason.

B. Temperature dependence in T1Q and T2Q terminations

Temperature dependence of band structure at T1Q and T2Q terminations are shown in Fig. 3. For the T1Q termination, a band hybridization is detected both above and below the transition temperature around 0.3 eV below the Fermi energy. Note that the outer weak intensity band in T1Q termination, marked as * in Figs. 3(a) and 3(b), may be the superposition of T2Q termination. Noticeable difference of energy dispersion between T1Q and T2Q terminations are the width of the strong linear surface band around 0.3 eV below the Fermi energy. The T2Q termination has larger width than the T1Q termination. In addition, the T2Q termination demonstrates an interesting band splitting below the transition temperature as

indicated by black arrows in Figs. 3(e) and 3(f). Such splitting of the top bulk valence band is due to the magnetic exchange splitting and has a larger size in the calculation for the ideal AFM as shown in Figs. 3(i) and 3(j). To distinguish the surface bands from the bulk bands, we also plotted the surface-only contributions in Figs. 3(e), 3(f), 3(k), and 3(l).

IV. CONCLUSION

In conclusion, we have demonstrated that $MnBi_6Te_{10}$ is one of the simplest intrinsic magnetic topological materials, making it a very promising platform to explore topological magnetic phenomena. Our studies demonstrate TRS-protected TI behavior at high temperatures and intrinsic AFM axion insulating behavior at low temperatures. Future work on tuning the Fermi level at the gap by chemical doping $MnBi_6Te_{10}$ should provide a pathway to study exciting TME effects, including a half-quantized surface anomalous Hall conductivity.

APPENDIXES

1. Methods

Single crystals of $MnBi_6Te_{10}$ were grown using Bi-Te as flux following the procedure described in Ref. [18]. Samples used for ARPES measurements were cleaved *in situ* at 40 K or 3.8 K in ultrahigh vacuum. The data were acquired using a tunable VUV laser ARPES system that consists of a Scienta Omicron DA30 electron analyzer, a picosecond Ti:Sapphire oscillator, and fourth-harmonic generator [45]. Data were collected using photon energy of 6.7 eV. Momentum and energy resolutions were set at ∼0.005 Å^{-1} and 2 meV. The diameter of the photon beam on the sample was ∼30 μm.

Band structures with SOC in DFT [46,47] have been calculated with van der Waals exchange-correlation functional DF1-optB86b [48,49], a plane-wave basis set, and projected augmented wave method [50] as implemented in VASP [51,52]. To account for the half-filled strongly localized Mn 3d orbitals, a Hubbard-like U [53] value of 3.0 eV is used. For bulk band structure of A-type anti-ferromagnetic (AFMA) $MnBi_6Te_{10}$, the rhombohedral unit cell is doubled along the c direction with a Monkhorst-Pack [54] (9×9×3) k-point mesh including the Γ point and a kinetic energy cutoff

of 270 eV. Experimental lattice constants [55] have been used with atomic positions relaxed until the absolute value of force on each atom is less than 0.02 eV/Å. A tight-binding model based on maximally localized Wannier functions [56–58] was constructed to closely reproduce the bulk band structure including SOC in the range of $E_F \pm 1$ eV with Mn sd, Bi p, and Te p orbitals [59]. Then the spectral functions and Fermi surface of a semi-infinite MnBi$_6$Te$_{10}$ (001) surface with different terminations were calculated with the surface Green'âs function methods [60–63] as implemented in WANNIERTOOLS [64]. The surface-only contribution for spectral function can be obtained by subtracting the imaginary part of the bulk Green's function from that of the surface Green's function.

2. Classification details

We here discuss a few more details on the evaluation of the band structure. As noticed by early work on magnetic TIs [37], inversion I eigenvalues reduce the problem of characterizing the band structure to simply evaluating the parity eigenvalues at the TRIM. In particular, if the total number of odd (−1) parties at the TRIM amounts to an odd number, the systems cannot be insulating. Similarly, if the system is insulating and has vanishing Chern numbers, the parity distribution conveys whether a θ term, with $\theta = \pi$ due to I symmetry, can be defined. The value of π is then attained if the total number of odd parity eigenvalue states add to twice an odd number. These evaluations are in essence generalizations of the Fu-Kane criterion [31], which states that the TRS-induced $\mathbf{Z}_2$ invariant ν is given by

$$(-1)^\nu = \prod_i \delta_i \quad \delta_i = \prod_m \xi_{2m}(\Gamma_i), \quad (A1)$$

where one evaluates the parity eigenvalues ξ of one of the *Kramer's pairs* of the $2m$ filled bands over the TRIM Γ_i, rather than individual bands as in the following paragraph. For the single band inversion at the Γ point, this thus gives the simplest configuration possible for obtaining a TRS protected TI. Recently, a lot of progress has been made by considering irreps at high-symmetry points in a very similar manner [34,35,65], as these gluing conditions map out a space of all possible band structures that can then be compared to Fourier transforms of atomic band structures that by definition span

the space of trivial insulators [32,33,36]. When regarded as vector spaces, dividing out the trivial subspace then results in quantities that can diagnose topology arising from the underlying space-group symmetry [32,33,36].

As motivated in the main text, the outcomes of parity distribution can be diagnosed in the general light of these symmetry-indicator developments by the quantity η:

$$\eta = 1/2 \sum_{\Gamma_i} n_{\mathbf{k}}^+ - n_{\mathbf{k}}^- \quad \mod 4. \quad (A2)$$

Indeed, the odd values identify Weyl semimetals, as these parity configurations show that Billouin zone cuts of different Chen number are connected, whereas 0 indicates a trivial insulator. The value of 2 can give rise to $\theta = \pi$ as it corresponds to a distribution of parity eigenvalues that amounts to twice an odd integer number η. We nonetheless emphasize that this in general can also indicate a stacked Chern insulator [37], for example, along the z direction with Chern number $C = 1$ in the $k_z = 0, \pi$ planes. It is the additional presence of the S symmetry that ensures pairing and indicates that the axion possibility is realized. This is because the presence of S symmetry ensures *pairing* at TRIM, eliminating the stacked Chern insulator. At $\tilde{k} = \pi$, S and I anticommute and result in pairs of opposite parity eigenvalue that are of no importance for the characterization, while at $\tilde{k} = 0$ these symmetries commute and thus ensure that the parity eigenvalues come as doubles of the same parity [33]. As a result, we observe that the classification gets reduced to the anticipated $\mathbf{Z}_2$ index, which is nontrivial due to the inverted pair at the Γ point, showing that the system is a quantized axion ($\theta = \pi$) insulator. Apart from the discussion on the presence of an axion term, we note for completeness that having zero Chern numbers and indicator $\eta = 2$ can also be associated with a higher order TI variant in absence of S symmetry, that is, in the $\mathbf{Z}_4$ perspective, and can thus in principle be accessed by breaking this symmetry. Physically, this case again requires altering the specific configuration of parity eigenvalues, in particular, the opposite pairing on the $\tilde{k} = \pi$ plane. Namely, breaking the symmetry between the layers related by S leaves behind a protected chiral 1D mode [33].

We point out that this indicator can trivially be rewritten into many other incarnations appearing recently. Using that the total number of occupied bands $n = n_{\mathbf{k}}^+ + n_{\mathbf{k}}^-$, which are
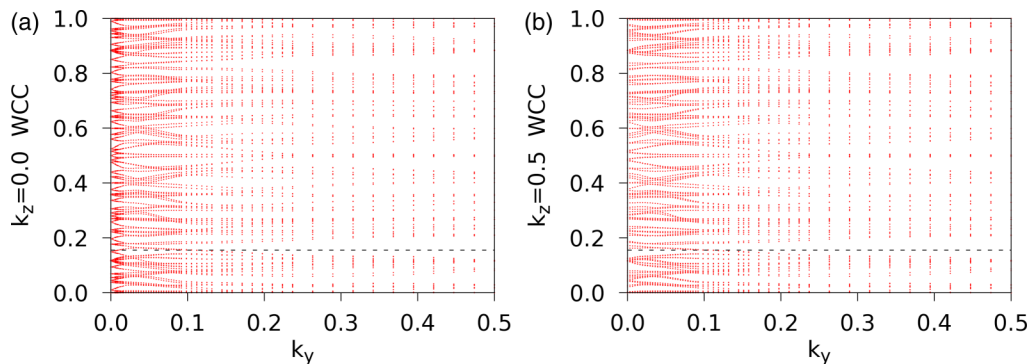

FIG. 4. Band topology: Wannier charge centers. Evolution of Wannier charge centers (WCCs) or Wilson loops for A-type AFM MnBi$_6$Te$_{10}$ on (a) $k_z = 0.0$ and (b) $k_z = 0.5$ plane. The 2D topological index is 1 and 0 in (a) and (b), respectively, because of odd and even numbers of crossing by the horizontal dashed line. The overall Z2 topological index is 1 in the TRS-protected TI context.
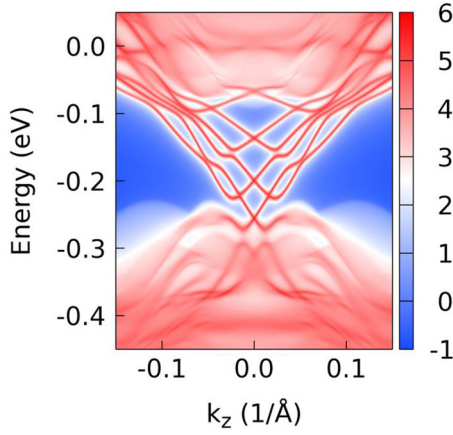
FIG. 5. DFT calculation of S-preserving surface. Spectral function along k_z direction on (110) surface of A-type AFM MnBi$_6$Te$_{10}$ showing the gapless surface Dirac cone for S-preserving surface.

assumed to be gapped at least at the TRIM, is independent of **k** and the number of TRIMs is eight, we can express the above quantity in $n_{\mathbf{k}}^+$ or $n_{\mathbf{k}}^-$ up to a number that is an integer multiple of four. In particular, by expressing the indicator in terms of $n_{\mathbf{k}}^+$, we arrive at

$$Z_4 = \sum_{occ} \sum_{\Gamma_i} \frac{1 + \xi_n(\Gamma_i)}{2} \quad \text{mod } 4, \qquad (A3)$$

where ξ refers to the parity eigenvalue of the nth occupied state.

We note that this characterization can generally be applied to I symmetric systems, in particular, ferromagnetic systems. Crucially, however, the AFM system at hand comes with the S symmetry that, as explained, collapses the classification index to $\mathbf{Z}_2$. This is, in particular, important for the bulk-boundary correspondence [66–70]. Indeed, the protecting inversion is naturally broken at the edge and hence gapless edge states are not guaranteed in that case. In this sense, the AFM

system is more analogous to a TRS-protected TI that also has I symmetry. The latter can diagnose the Z_2 classification coming from TRS by the parity distribution. Surfaces that preserve TRS nonetheless have gapless states. Similarly, in the AFM axion insulator, the parties diagnose the θ term, but the $\mathbf{Z}_2$ index comes from the S symmetry. As a consequence, gapped edges states only occur on S-breaking surfaces, see also the next section.

Finally, to further underpin our analysis, we have also constructed the Wilson Flows, see Fig. 4. As demonstrated in a series of works [71–75], invariants can generally be deduced from the winding in (nested) Wilson spectra. Heuristically, this is because they track the flow of the Wannier centers. As consistent with the previously outlined classification analysis, we find a Wilson winding in the $\tilde{k} = 0$ plane but not in the $\tilde{k} = \pi$ plane.

3. DFT calculation on (110) surface

Figure 5 shows a DFT calculation of A-type AFM MnBi$_6$Te$_{10}$ on the (110) surface, where S symmetry is preserved. Consistent with previous arguments, we observe a gapless surface Dirac cone, further underpinning our analysis.

4. DFT calculation of surface states on TS termination

Figure 6 is the DFT calculation results on the surface state only for TS termination.

5. Experimental details of the ARPES measurements

We used four single crystals of MnBi$_6$Te$_{10}$ for ARPES measurements; each of them was cleaved five separate times. All three surface terminations were found in each of the 20 cleaves. Due to the small beam size, each termination could be quite well isolated and measured separately, although the T1Q termination seems to have slight contamination with the T2Q signal, likely due to the presence of small islands. T1Q termination was more rare than the other ones. We
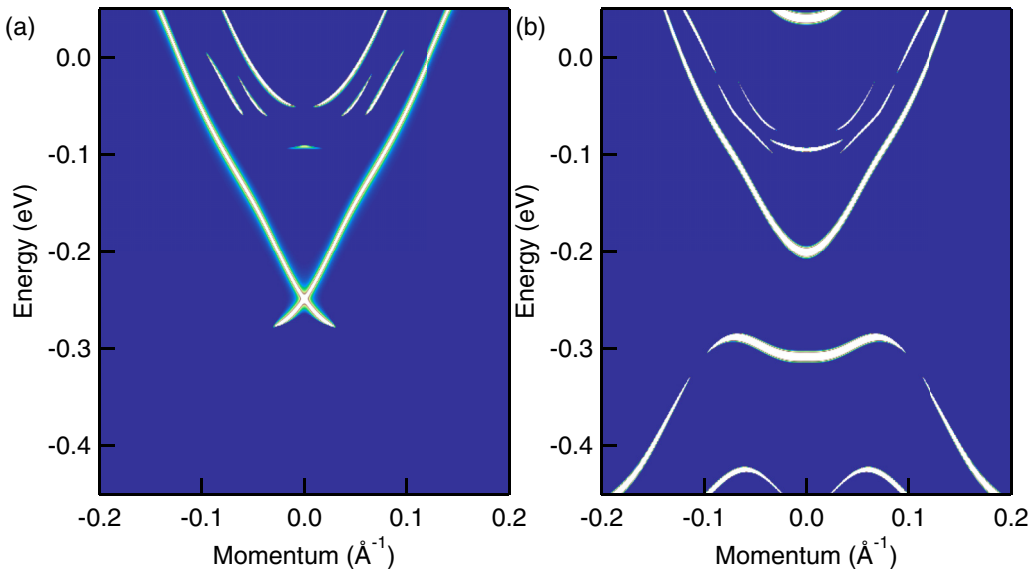

FIG. 6. Only surface states (without bulk bands) for TS termination in Figs. 2(c) and 2(d).
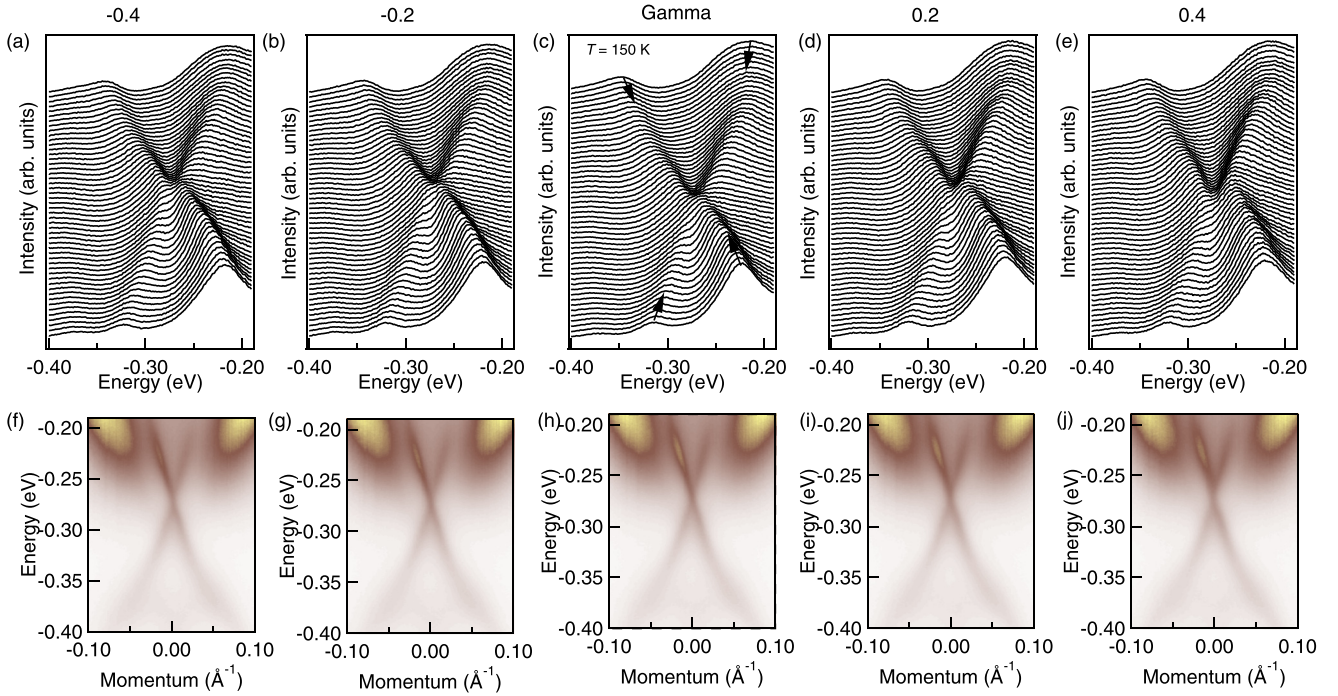
T = 150 K

FIG. 7. Band dispersion near Γ point at $T = 150$ K (a)–(e) EDCs at $T = 150$ K near the Γ point; $-0.4°$ from Γ, $-0.2°$ from Γ, Γ, $0.2°$ from Γ, and $0.4°$ from Γ. (f)–(j) Band dispersion at $T = 150$ K near the Γ point; $-0.4°$ from Γ, $-0.2°$ from Γ, Γ, $0.2°$ from Γ, and $0.4°$ from Γ.

noticed a slight variation of the the E_F and the size of the low-temperature gap within the TS termination. This may be due to the presence of steps to adjacent terminations or small variations of sample chemistry. Samples were cleaved at $T = 3.8$ K three times to make sure the gap for the TS termination and the splitting for the T2Q termination at low temperatures is intrinsic and not due to spurious effects such as surface aging. Due to the Dirac cone-shaped surface band,
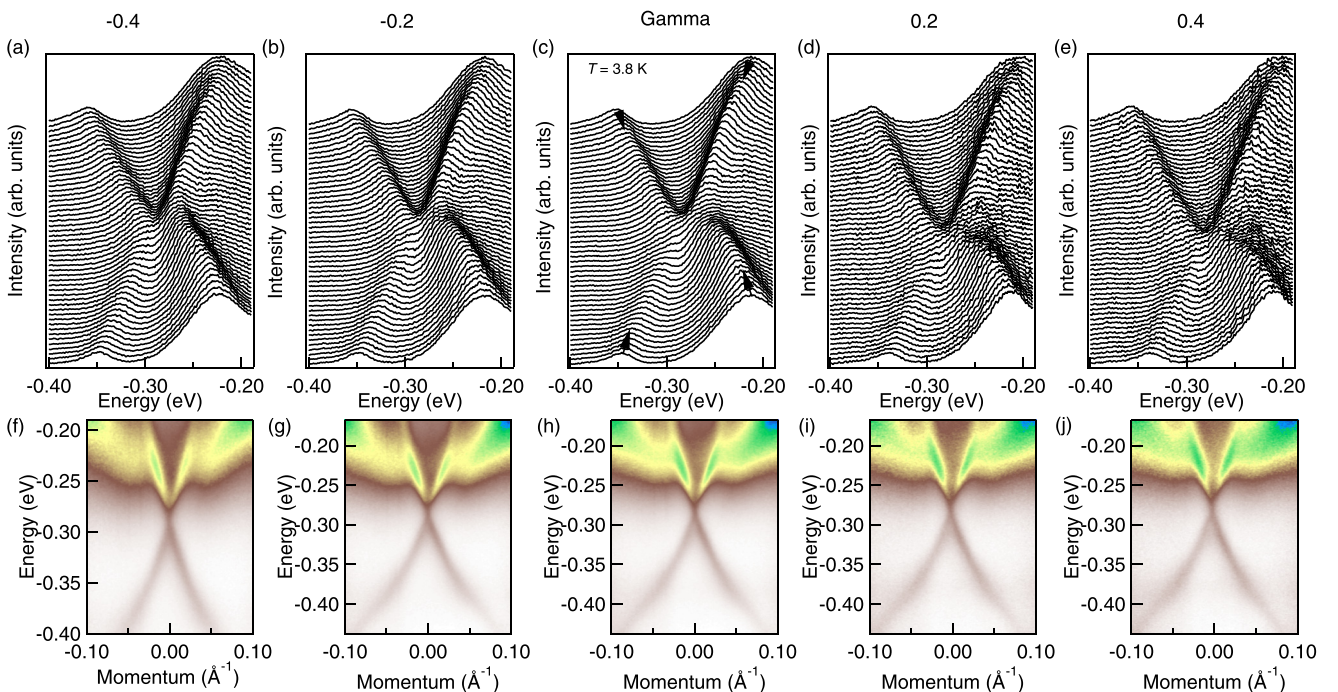
T = 3.8 K

FIG. 8. Band dispersion near Γ point at $T = 3.8$ K (a)–(e) EDCs at $T = 3.8$ K near the Γ point; $-0.4°$ from Γ, $-0.2°$ from Γ, Γ, $0.2°$ from Γ, and $0.4°$ from Γ. (f)–(j) Band dispersion at $T = 3.8$ K near the Γ point; $-0.4°$ from Γ, $-0.2°$ from Γ, Γ, $0.2°$ from Γ, and $0.4°$ from Γ.

even a small misalignment from Γ will manifest itself as an apparent gap. Such misalignment is relatively easy to occur in the experiment as the sample surface is not perfectly flat and small movements (e.g., due to thermal expansion then changing temperature) can change the angular orientation of surface normal. We therefore took extraordinary care to perform very fine angular scans for each measurement. Those are illustrated in Figs. 7 and 8. High-temperature data exactly at Γ Fig. 7(c) shows merging of the upper and lower bands and gapless Dirac state. For even small changes of lateral

momentum away from Γ (i.e., emission angle from normal), there is clearly a visible separation between the upper and lower cones, which may be misinterpreted as a gap. At low temperatures, Fig. 8, the upper and lower cones are separated at Γ and this separation increases away from Γ. This is definite proof for the presence of an energy gap at low temperatures.

To have energy dispersions at Γ, we performed the theta scan $\Gamma \pm \sim 1^\text{o}$ with 0.2 $^\text{o}$ step size for all temperatures. Figures 7 and 8 show the selective theta scan for $T = 3.8$ K and 150 K.

[1] X.-L. Qi, T. L. Hughes, and S.-C. Zhang, Phys. Rev. B **78**, 195424 (2008).

[2] F. Wilczek, Phys. Rev. Lett. **58**, 1799 (1987).

[3] A. M. Essin, J. E. Moore, and D. Vanderbilt, Phys. Rev. Lett. **102**, 146805 (2009).

[4] X.-L. Qi, R. Li, J. Zang, and S.-C. Zhang, Science **323**, 1184 (2009).

[5] E. Witten, Phys. Lett. B **86**, 283 (1979).

[6] M.-C. Chang and M.-F. Yang, Phys. Rev. B **80**, 113304 (2009).

[7] J. Maciejko, X.-L. Qi, H. D. Drew, and S.-C. Zhang, Phys. Rev. Lett. **105**, 166803 (2010).

[8] W.-K. Tse and A. H. MacDonald, Phys. Rev. Lett. **105**, 057401 (2010).

[9] L. Wu, M. Salehi, N. Koirala, J. Moon, S. Oh, and N. P. Armitage, Science **354**, 1124 (2016).

[10] X. Wan, A. M. Turner, A. Vishwanath, and S. Y. Savrasov, Phys. Rev. B **83**, 205101 (2011).

[11] X. Wan, A. Vishwanath, and S. Y. Savrasov, Phys. Rev. Lett. **108**, 146601 (2012).

[12] S. Coh and D. Vanderbilt, Phys. Rev. B **88**, 121106(R) (2013).

[13] E. Y. Ma, Y.-T. Cui, K. Ueda, S. Tang, K. Chen, N. Tamura, P. M. Wu, J. Fujioka, Y. Tokura, and Z.-X. Shen, Science **350**, 538 (2015).

[14] D. Zhang, M. Shi, T. Zhu, D. Xing, H. Zhang, and J. Wang, Phys. Rev. Lett. **122**, 206401 (2019).

[15] J. Li, Y. Li, S. Du, Z. Wang, B.-L. Gu, S.-C. Zhang, K. He, W. Duan, and Y. Xu, Sci. Adv. **5**, eaaw5685 (2019).

[16] J.-Q. Yan, Q. Zhang, T. Heitmann, Z. Huang, K. Y. Chen, J.-G. Cheng, W. Wu, D. Vaknin, B. C. Sales, and R. J. McQueeney, Phys. Rev. Mater. **3**, 064202 (2019).

[17] M. Z. Shi, B. Lei, C. S. Zhu, D. H. Ma, J. H. Cui, Z. L. Sun, J. J. Ying, and X. H. Chen, Phys. Rev. B **100**, 155144 (2019).

[18] J.-Q. Yan, Y. H. Liu, D. S. Parker, Y. Wu, A. A. Aczel, M. Matsuda, M. A. McGuire, and B. C. Sales, Phys. Rev. Materials **4**, 054202 (2020).

[19] L. Ding, C. Hu, F. Ye, E. Feng, N. Ni, and H. Cao, Phys. Rev. B **101**, 020412(R) (2020).

[20] Y. Deng, Y. Yu, M. Z. Shi, Z. Guo, Z. Xu, J. Wang, X. H. Chen, and Y. Zhang, Science **367**, 895 (2020).

[21] C. Hu, L. Ding, K. N. Gordon, B. Ghosh, H. Li, S.-W. Lian, A. G. Linn, H.-J. Tien, C.-Y. Huang, P. V. S. Reddy, B. Singh, A. Agarwal, A. Bansil, S.-Y. Xu, H. Lin, H. Cao, T.-R. Chang, D. Dessau, and N. Ni, arXiv:1910.12847.

[22] M. M. Otrokov, I. I. Klimovskikh, H. Bentmann, A. Zeugner, Z. S. Aliev, S. Gass, A. U. Wolter, A. V. Koroleva, D. Estyunin, A. M. Shikin et al., Nature **576**, 416 (2019).

[23] A. Zeugner, F. Nietschke, A. U. B. Wolter, S. Gaß, R. C. Vidal, T. R. F. Peixoto, D. Pohl, C. Damm, A. Lubk, R. Hentrich, S. K. Moser, C. Fornari, C. H. Min, S. Schatz, K. Kißner, M. Ünzelmann, M. Kaiser, F. Scaravaggi, B. Rellinghaus, K. Nielsch, C. Hess, B. Büchner, F. Reinert, H. Bentmann, O. Oeckler, T. Doert, M. Ruck, and A. Isaeva, Chem. Mater. **31**, 2795 (2019).

[24] S. H. Lee, Y. Zhu, Y. Wang, L. Miao, T. Pillsbury, H. Yi, S. Kempinger, J. Hu, C. A. Heikes, P. Quarterman, W. Ratcliff, J. A. Borchers, H. Zhang, X. Ke, D. Graf, N. Alem, C.-Z. Chang, N. Samarth, and Z. Mao, Phys. Rev. Research **1**, 012011 (2019).

[25] R. C. Vidal, H. Bentmann, T. R. F. Peixoto, A. Zeugner, S. Moser, C.-H. Min, S. Schatz, K. Kißner, M. Ünzelmann, C. I. Fornari, H. B. Vasili, M. Valvidares, K. Sakamoto, D. Mondal, J. Fujii, I. Vobornik, S. Jung, C. Cacho, T. K. Kim, R. J. Koch, C. Jozwiak, A. Bostwick, J. D. Denlinger, E. Rotenberg, J. Buck, M. Hoesch, F. Diekmann, S. Rohlf, M. Kalläne, K. Rossnagel, M. M. Otrokov, E. V. Chulkov, M. Ruck, A. Isaeva, and F. Reinert, Phys. Rev. B **100**, 121104(R) (2019).

[26] P. Swatek, Y. Wu, L.-L. Wang, K. Lee, B. Schrunk, J. Yan, and A. Kaminski, Phys. Rev. B **101**, 161109(R) (2020).

[27] C. Hu, K. N. Gordon, P. Liu, J. Liu, X. Zhou, P. Hao, D. Narayan, E. Emmanouilidou, H. Sun, Y. Liu, H. Brawer, A. P. Ramirez, L. Ding, H. Cao, Q. Liu, D. Dessau, and N. Ni, Nat. Commun. **11**, 97 (2020).

[28] Y.-J. Hao, P. Liu, Y. Feng, X.-M. Ma, E. F. Schwier, M. Arita, S. Kumar, C. Hu, R. Lu, M. Zeng et al., Phys. Rev. X **9**, 041038 (2019).

[29] Y. J. Chen, L. X. Xu, J. H. Li, Y. W. Li, H. Y. Wang, C. F. Zhang, H. Li, Y. Wu, A. J. Liang, C. Chen, S. W. Jung et al., Phys. Rev. X **9**, 041040 (2019).

[30] H. Li, S.-Y. Gao, S.-F. Duan, Y.-F. Xu, K.-J. Zhu, S.-J. Tian, J.C. Gao, W.-H. Fan, Z.-C. Rao, J.-R. Huang, J.-J. Li et al., Phys. Rev. X **9**, 041039 (2019).

[31] L. Fu and C. L. Kane, Phys. Rev. B **76**, 045302 (2007).

[32] H. C. Po, A. Vishwanath, and H. Watanabe, Nat. Commun. **8**, 50 (2017).

[33] H. Watanabe, H. C. Po, and A. Vishwanath, Sci. Adv. **4**, eaat8685 (2018).

[34] R.-J. Slager, A. Mesaros, V. Juričić, and J. Zaanen, Nat. Phys. **9**, 98 (2012).

[35] J. Kruthoff, J. de Boer, J. van Wezel, C. L. Kane, and R.-J. Slager, Phys. Rev. X **7**, 041069 (2017).

[36] B. Bradlyn, L. Elcoro, J. Cano, M. G. Vergniory, Z. Wang, C. Felser, M. I. Aroyo, and B. A. Bernevig, Nature **547**, 298 (2017).

[37] A. M. Turner, Y. Zhang, R. S. K. Mong, and A. Vishwanath, Phys. Rev. B **85**, 165120 (2012).

[38] T. L. Hughes, E. Prodan, and B. A. Bernevig, Phys. Rev. B **83**, 245132 (2011).

[39] H. Zhang, C.-X. Liu, X.-L. Qi, X. Dai, Z. Fang, and S.-C. Zhang, Nat. Phys. **5**, 438 (2009).

[40] R. S. K. Mong, A. M. Essin, and J. E. Moore, Phys. Rev. B **81**, 245209 (2010).

[41] N. Varnava and D. Vanderbilt, Phys. Rev. B **98**, 245117 (2018).

[42] M. Papagno, S. V. Eremeev, J. Fujii, Z. S. Aliev, M. B. Babanly, S. Kr. Mahatha, I. Vobornik, N. T. Mamedov, D. Pacilé, and E. V. Chulkov, ACS Nano **10**, 3518 (2016).

[43] D. Mou, A. Sapkota, H.-H. Kung, V. Krapivin, Y. Wu, A. Kreyssig, X. Zhou, A. I. Goldman, G. Blumberg, R. Flint, and A. Kaminski, Phys. Rev. Lett. **116**, 196401 (2016).

[44] DOI: 10.18126/285a-7ael.

[45] R. Jiang, D. Mou, Y. Wu, L. Huang, C. D. McMillen, J. Kolis, H. G. Giesber, J. J. Egan, and A. Kaminski, Rev. Sci. Instrum. **85**, 033902 (2014).

[46] P. Hohenberg and W. Kohn, Phys. Rev. **136**, B864 (1964).

[47] W. Kohn and L. J. Sham, Phys. Rev. **140**, A1133 (1965).

[48] M. Dion, H. Rydberg, E. Schröder, D.C. Langreth, and B. I. Lundqvist, Phys. Rev. Lett. **92**, 246401 (2004).

[49] J. Klimeš, D. R. Bowler, and A. Michaelides, Phys. Rev. B **83**, 195131 (2011).

[50] P. E. Blöchl, Phys. Rev. B **50**, 17953 (1994).

[51] G. Kresse and J. Furthmüller, Phys. Rev. B **54**, 11169 (1996).

[52] G. Kresse and J. Furthmüller, Comput. Mater. Sci. **6**, 15 (1996).

[53] S. L. Dudarev, G. A. Botton, S. Y. Savrasov, C. J. Humphreys, and A. P. Sutton, Phys. Rev. B **57**, 1505 (1998).

[54] H. J. Monkhorst and J. D. Pack, Phys. Rev. B **13**, 5188 (1976).

[55] Z. S. Aliev, I. R. Amiraslanov, D. I. Nasonova, A. V. Shevelkov, N. A. Abdullayev, Z. A. Jahangirli, E. N. Orujlu, M. M. Otrokov, N. T. Mamedov, M. B. Babanly *et al.*, J. Alloys Compd. **789**, 443 (2019).

[56] N. Marzari and D. Vanderbilt, Phys. Rev. B **56**, 12847 (1997).

[57] I. Souza, N. Marzari, and D. Vanderbilt, Phys. Rev. B **65**, 035109 (2001).

[58] N. Marzari, A. A. Mostofi, J. R. Yates, I. Souza, and D. Vanderbilt, Rev. Mod. Phys. **84**, 1419 (2012).

[59] M. M. Otrokov, I. P. Rusinov, M. Blanco-Rey, M. Hoffmann, A. Y. Vyazovskaya, S. V. Eremeev, A. Ernst, P. M. Echenique, A. Arnau, and E. V. Chulkov, Phys. Rev. Lett. **122**, 107202 (2019).

[60] D. H. Lee and J. D. Joannopoulos, Phys. Rev. B **23**, 4988 (1981).

[61] D. H. Lee and J. D. Joannopoulos, Phys. Rev. B **23**, 4997 (1981).

[62] M. P. L. Sancho, J. M. L. Sancho, and J. Rubio, J. Phys. F: Met. Phys. **14**, 1205 (1984).

[63] M. P. Lopez Sancho, J. M. Lopez Sancho, J. M. L. Sancho, and J. Rubio, J. Phys. F: Met. Phys. **15**, 851 (1985).

[64] Q. Wu, S. Zhang, H.-F. Song, M. Troyer, and A. A. Soluyanov, Comput. Phys. Commun. **224**, 405 (2018).

[65] R.-J. Slager, J. Phys. Chem. Solids **128**, 24 (2019).

[66] J.-W. Rhim, J. H. Bardarson, and R.-J. Slager, Phys. Rev. B **97**, 115143 (2018).

[67] R.-J. Slager, V. Juričić, and B. Roy, Phys. Rev. B **96**, 201401(R) (2017).

[68] R.-J. Slager, V. Juričić, V. Lahtinen, and J. Zaanen, Phys. Rev. B **93**, 245406 (2016).

[69] Y. Hatsugai, Phys. Rev. Lett. **71**, 3697 (1993).

[70] R.-J. Slager, L. Rademaker, J. Zaanen, and L. Balents, Phys. Rev. B **92**, 085126 (2015).

[71] A. A. Soluyanov and D. Vanderbilt, Phys. Rev. B **83**, 235401 (2011).

[72] A. Alexandradinata, X. Dai, and B. A. Bernevig, Phys. Rev. B **89**, 155114 (2014).

[73] R. Yu, X. L. Qi, A. Bernevig, Z. Fang, and X. Dai, Phys. Rev. B **84**, 075119 (2011).

[74] A. Bouhon, A. M. Black-Schaffer, and R.-J. Slager, Phys. Rev. B **100**, 195135 (2019).

[75] A. Bouhon and A. M. Black-Schaffer, Phys. Rev. B **95**, 241101(R) (2017).